Optimizing Cluster Size Through Handoff Analysis in User-Centric Cooperative Wireless Networks

Wei Bao, *Member, IEEE*, and Ben Liang, *Senior Member, IEEE*

***Abstract*— User-centric base station (BS) cooperation has been regarded as an effective solution for improving network coverage and throughput in next-generation wireless systems. However, it also introduces more complicated handoff patterns, which may potentially degrade user performance. In this paper, we aim to theoretically quantify the tradeoff between handoff cost and data rate. Two user-centric clustering modes are investigated: number-based cooperation (NBC), which is easier to implement, and distance-based cooperation (DBC), which gives higher data rate performance. In the NBC mode, a user is served by its K closest BSs, while in the DBC mode, it is served by all BSs within a given distance. However, due to the randomness of network topology, it is a challenging task to track handoffs and to characterize data rates. To address this issue, we propose a stochastic geometric analysis framework on user mobility, to derive a theoretical expression for the handoff rate experienced by an active user with arbitrary movement trajectory. Then, we characterize the average downlink user data rate under a common non-coherent joint-transmission scheme, which is used to illustrate the tradeoff between handoff rate and data rate in optimizing the cooperative cluster size. We conclude that in the NBC (resp. DBC) mode, the optimal cluster size is asymptotically inversely (resp. inversely) proportional to the square of the user speed and asymptotically inversely (resp. inversely) proportional to the BS intensity. Finally, computer simulation is conducted to validate the correctness and usefulness of our analysis.**

***Index Terms*— Cooperative network, stochastic geometry, handoff, mobility.**

I. Introduction

BASE station (BS) cooperation is expected to become an important feature in next-generation wireless networks [1]. It allows simultaneous connections from one user to multiple BSs, to significantly enhance the received power level and reduce interference. In addition, compared with the traditional single-BS association mode, users are less likely to enter a dead spot, e.g., near the cell edge, where the received signal-to-interference-plus-noise ratio (SINR) becomes too low.

A central element in the implementation of BS cooperation is BS clustering, where a set of BSs are selected to cooperatively serve a user. There are two types of BS clustering modes, namely the *disjoint clustering* and *user-centric clustering*. In the disjoint clustering mode, the entire geographical region of the network is partitioned into multiple non-overlapping subregions, and the BSs in each subregion cooperatively serve users within the subregion. In the user-centric clustering mode, each user is served by its individual cluster of neighboring BSs. As the user moves, its BS clusters are updated, so that each BS appears in different clusters. The user-centric clustering mode is more advantageous compared with its disjoint counterpart, since the BS clusters are continuously updated based on the user location, which avoids the low-SINR cluster edges that are artificially created in disjoint clustering. Consequently, in this work, we focus on the user-centric clustering mode.

The user-centric clustering mode can be further classified into the *number-based cooperation* (NBC) mode [2] and the *distance-based cooperation* (DBC) mode [3]. In the NBC mode, a user is served by its K closest BSs, while in the DBC mode, it is served by all BSs within a distance of R from it. The NBC mode is easier to implement in reality. This is because a user does not directly know its distances to BSs. It is much easier to measure the received power levels from BSs, but additional effort is needed to translate the received power levels to distances (e.g., via an accurate pathloss model). In the NBC mode, a user simply connects to the K BSs with the highest received power levels, without explicitly knowing the distances. In the DBC mode, since a user is served by BSs within a distance of R, the user needs to explicitly know its distances to nearby BSs. In addition, the NBC mode can avoid the possibility that a user is served by no BS when there is no BS within a distance of R from it. On the other hand, the DBC mode gives better data rate performance.[1] Both the NBC and DBC modes are studied in this work.

In the presence of user-centric BS cooperation, mobility management becomes more challenging. The handoff patterns are more complicated compared with those in traditional single-BS association systems, since the handoffs now involve changes in terms of a set of multiple BSs. Different from the single-BS association scenario, there are no explicit cells surrounding individual BSs. Instead, we need to characterize the *virtual cell*, which corresponds to the region where a user connects with the same set of BSs. If a user crosses the boundary between two virtual cells, its connected BS set is changed and a handoff is made. However, due to the spatial randomness of BSs as well as user-centric BS cooperation,

Manuscript received September 14, 2016; revised June 12, 2017 and October 25, 2017; accepted October 30, 2017. Date of publication November 14, 2017; date of current version February 9, 2018. This work was supported by grants from the Natural Sciences and Engineering Research Council of Canada. The associate editor coordinating the review of this paper and approving it for publication was B. Hamdaoui. *(Corresponding author: Wei Bao.)*

W. Bao is with the School of Information Technologies, The University of Sydney, Sydney, NSW 2006, Australia (e-mail: wei.bao@sydney.edu.au).

B. Liang is with the Department of Electrical and Computer Engineering, University of Toronto, Toronto, ON M5S3G4, Canada (e-mail: liang@comm.utoronto.ca).

Color versions of one or more of the figures in this paper are available online at http://ieeexplore.ieee.org.

Digital Object Identifier 10.1109/TWC.2017.2771343

[1] This will be shown in Section VI.

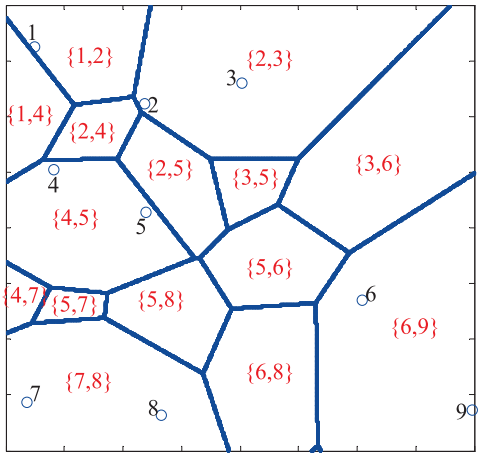

Fig. 1. An example of virtual cells in NBC mode. The numbers 1 to 9 indicate 9 BSs; $\{A, B\}$ indicates the virtual cell region served by BSs A and B.

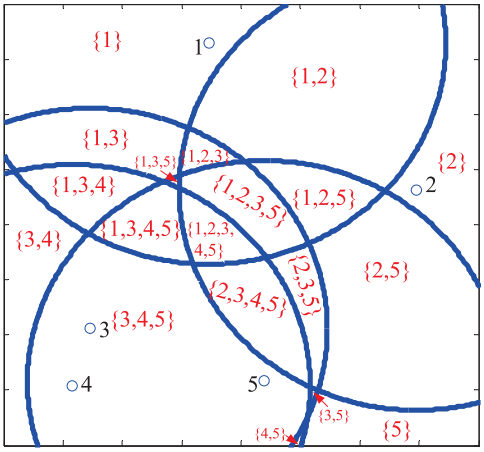

Fig. 2. An example of virtual cells in DBC mode. The numbers 1 to 5 indicate 5 BSs; $\{\cdot\}$ indicates the virtual cell region served by the set of BSs in brackets. Note that if an area is covered by many BSs (e.g., the area covered by BSs 1, 2, 3, 4, and 5), the area is likely to be far away from all of these BSs. In this area, one or two serving BSs are not enough to provide sufficiently strong signals, so that a greater number of cooperated BSs is desirable, i.e., all of BSs 1, 2, 3, 4, and 5 jointly serve this area. This feature is one advantage of the DBC mode. More BSs jointly serve the "dead spot" areas to improve the quality of signals in those areas.

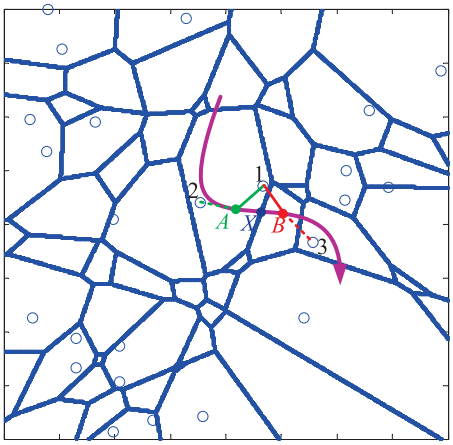

(a) A user is served by two closest BSs. It makes 4 handoffs. For example, it accesses BSs 1 and 2 at A, BSs 1 and 3 at B, and makes a handoff at X.

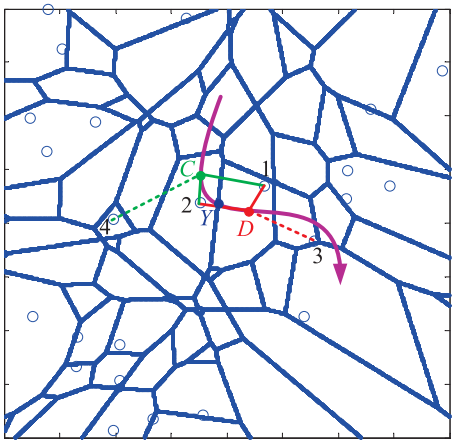

(b) Same BS locations and user trajectory as above. The user is served by three closest BSs. It makes 6 handoffs. For example, it accesses BSs 1, 2, and 4 at C, BSs 1, 2, and 3 at D, and makes a handoff at Y.

Fig. 3. A comparison between two-BS cooperation and there-BS cooperation. BSs are represented by circles; blue curves show virtual cell boundary; user trajectory is shown as the magenta arrow.

the virtual cells are generated randomly and irregularly. It is difficult to characterize the virtual cell boundary and to track boundary crossings made by users in the system. Fig. 1 shows an example topology where users are served by two closest BSs, while Fig. 2 shows the scenario where users are served by all BSs within a given distance. Previously developed techniques for single-BS handoff analysis [4]–[7] are insufficient to model the complex handoff patterns in such user-centric cooperative wireless networks.

Characterizing the handoff rate can provide important guidelines for system design. For example, optimizing the BS cluster size requires accounting for the impacts of both the handoff rate and the data rate. Consider the NBC example in Fig. 3, where an active user's trajectory is indicated by the magenta arrow. If the user is served by two closest BSs, it experiences 4 handoffs, as shown in Fig. 3(a). In contrast, as shown in Fig. 3(b), if the user is served by three cooperative BSs, it experiences 6 handoffs. However, in the latter case, the user could potentially experience a higher data rate since it is served by one more BS. A similar tradeoff between handoff and data rate arises when DBC is employed. Thus, an optimal system design must balance the tradeoff between a larger BS cluster to improve data rate and more frequent handoffs, which increases cost and potentially deteriorates service quality.

In this work, we propose a new stochastic geometric analysis framework to quantify the handoff rate in a user-centric cooperative wireless network, where either the NBC or DBC mode is applied. We model the BSs as a Poisson point process (PPP) to capture their spatial randomness. Our contributions are as follows:

- In both the NBC and DBC modes, through stochastic and analytic geometric analysis, we derive an exact expression for the handoff rate experienced by an active user with arbitrary movement trajectory.
- As a study on the application of the above handoff rate analysis, after calculating the average downlink

data rate of users under the non-coherent joint-transmission (NC-JT) scheme, we further investigate the optimal cluster size in both the NBC and DBC modes,[2] to balance the tradeoff between handoff rate and data rate. In the NBC (resp. DBC) mode, the optimal cluster size is asymptotically inversely (resp. inversely) proportional to the square of the user speed and asymptotically inversely (resp. inversely) proportional to the BS intensity.
- Computer simulation is conducted to validate the correctness and usefulness of our analysis, through which we also show that the handoff rate derived under the PPP assumption provides close approximations even if the BSs are non-PPP distributed.

The rest of this paper is organized as follows. In Section II, we discuss the relation between our work and prior works. In Section III, we present the system model. In Section IV, we present the theoretical analysis on the handoff rate in the system. In Section V, we study the optimal cluster size as an application scenario. In Section VI, we validate our analysis with simulation. Finally, conclusions are given in Section VII.

II. Related Work

In this section, we summarize the prior research in stochastic geometric modeling of cooperative wireless networks, and the existing techniques for handoff analysis.

A. Stochastic Geometric Analysis of Cooperative Wireless Networks

In order to capture the spatial randomness of BSs and users, analysis techniques based on the theory of stochastic geometry have been applied to evaluate performance metrics such as interference distribution, coverage probability, data rate, and throughput in cooperative wireless networks. In these works, the BSs are often assumed to be spatially distributed as a PPP. In [8], a two-BS cooperation model was proposed and the user coverage probability was derived for this model. In [9]–[11], various forms of the disjoint clustering mode of BS cooperation were studied. In [2], [3], and [12]–[15], the performance of different joint transmission schemes in user-centric BS cooperation was evaluated, including NC-JT [3], [12], synchronous joint transmission [13], interference nulling [14], and coordinated beamforming [2], [15]. All of these works focused only on networks with stationary users, and thus handoffs were not studied.

B. Handoff Analysis in Wireless Cellular Networks

In the scope of handoff analysis, all previous works concerned only the single-BS association scenario. One well-known category of analysis techniques employ queueing formulation, without explicitly modeling the geometric patterns of cell shapes in the networks [16]–[19]. In these works, cells were modeled as queues containing active users, and handoffs were modeled as unit transfers between queues. Another common category of analysis techniques assume regularly grided cells for mathematical convenience. Examples of such geometric topologies include hexagonal grids [20], [21], square grids [22], and circles overlaying hexagons [23].

To further capture the spatial randomness of network topologies, a seminal study on user mobility was conducted in [4] for a single-tier cellular network with randomly distributed BSs, where the BSs were modeled as a homogeneous PPP, and cell splitting was modeled as a standard Poisson Voronoi. The case of multi-tier cellular networks was considered in [5] and [6], where each tier of BSs was modeled as a homogeneous PPP, and the resultant cell splitting was modeled as a weighted Poisson Voronoi. Further extension to [5] was given in [7], where the BS tiers were modeled as Poisson cluster processes (PCPs), such that their aggregation around highly populated areas could be accommodated. However, the above works considered only single-BS association, which is not applicable to BS cooperative wireless networks.

A preliminary version of this work was presented in [24], where only the NBC case was considered. The new contribution of the DBC analysis in this paper is major. This is because the cell splitting of DBC is completely different from that of NBC, which leads to substantially different analysis in handoff rates and data rates, as well as the subsequent analysis on the optimal cluster size. These new analytical results also enable a quantitative comparison between NBC and DBC. The current version also contains substantial further analytical details, simulation results, and discussion.

III. System Model

In this section, we describe the user-centric cooperative network under consideration, clarifying the notions of user handoffs and virtual cells.

A. User-Centric Cooperative Wireless Network

We consider a single-tier wireless system with BSs scattered in the two-dimensional Euclidean space $\mathbb{R}^2$ according to a homogeneous Poisson point process (PPP) Φ with intensity λ. The PPP assumption is commonly adopted in stochastic geometric analysis in the research literature [2], [3], [12]–[15], [25], [26, Part 2], [27, Part 4], [28, Sec. 5]. We additionally show through simulation in Section VI that our results derived under the PPP assumption provide close approximations even when BSs are non-PPP distributed.

In both modes, let K denote the cluster size. In the NBC mode, each user is served by its K closest BSs, where the minimum value of K is $K_{\min} = 2$. In the DBC mode, each user is served by all BSs within a range of R from it. We define $K = \pi R^2 \lambda$, which is the expected number of serving BSs. There is a one-to-one mapping between R and K.

Note that in both modes, we do not need to specify the transmission scheme for handoff analysis, so that this model is applicable to many different scenarios, such as NC-JT, cooperative beamforming, and cloud radio access network (C-RAN).

[2]In the NBC mode, the cluster size is defined as K (i.e., the number of cooperative BSs). In the DBC mode, the number of cooperative BSs is a random variable. The cluster size is defined as the average number of cooperative BSs. See Section III-A for details.

B. Handoffs in User-Centric Cooperative Wireless Network

A handoff is defined as the event that the connected BS set of an active user is changed. One major goal of this work is to quantify the rate of handoffs of some active user moving in the network. Therefore, we need to characterize the *virtual cell*, defined as the region in which a user is served by the same set of BSs. In the NBC mode, the overall virtual cells correspond to a Kth-order Poisson Voronoi [2], [8], an example of which is shown in Fig. 1. Let $\mathbf{T}_K^{(1)}$ denote the overall set of cell boundaries of the Kth-order Poisson Voronoi. Whenever an active user crosses $\mathbf{T}_K^{(1)}$, the set of connected BSs are changed, and thus a handoff is made. In the DBC mode, let $\Xi_R^{(1)}$ denote the overall set of virtual cell boundaries under R.

Let $\mathcal{T}_0$ denote the trajectory of the user, which is of finite length. The number of handoffs the user experiences in the NBC mode (resp. DBC mode) is equal to the number of intersections between $\mathcal{T}_0$ and $\mathbf{T}_K^{(1)}$ (resp. $\Xi_R^{(1)}$), which is denoted by $\mathcal{N}(\mathcal{T}_0, \mathbf{T}_K^{(1)})$ (resp. $\mathcal{N}(\mathcal{T}_0, \Xi_R^{(1)})$).

C. Virtual Cell Boundaries

1) Kth-Order Poisson Voronoi in NBC Mode: We formally define $\mathbf{T}_K^{(1)}$ as follows. Let $\mathcal{C} = \{\mathbf{x}_1, \ldots, \mathbf{x}_K\} \subset \Phi$ denote a set of K BSs. The Kth-order Voronoi cell with respect to the BS set $\mathcal{C}$ is defined as the set of points closer to $\mathbf{x}_1, \ldots, \mathbf{x}_K$ than any other points in Φ, i.e.,

$$\mathcal{V}(\mathcal{C}) = \{\mathbf{y} \in \mathbb{R}^2 \big| \forall \mathbf{x} \in \mathcal{C}, \mathbf{x}' \in \Phi \backslash \mathcal{C}, |\mathbf{y} - \mathbf{x}| \leq |\mathbf{y} - \mathbf{x}'|\}. \quad (1)$$

In other words, the distance from an arbitrary point in $\mathcal{V}(\mathcal{C})$ to any BS in $\mathcal{C}$ is no larger than the distance from the point to any BS not in $\mathcal{C}$. Note that a BS may not be in the cell formed by itself. For example, in Fig. 1, neither BS 6 nor BS 8 is inside the region served by BSs $\{6, 8\}$. We also note that for some $\mathcal{C}$, $\mathcal{V}(\mathcal{C}) = \emptyset$. In Fig. 1, nowhere is served by BSs $\{1, 9\}$.

Thus, $\mathbf{T}_K^{(1)}$ corresponds to the set of points on $\mathbb{R}^2$ which belongs to two different cells:

$$\mathbf{T}_K^{(1)} = \{\mathbf{y} \in \mathbb{R}^2 \big| \exists \mathcal{C} \neq \mathcal{C}', \text{s.t. } \mathbf{y} \in \mathcal{V}(\mathcal{C}) \bigcap \mathcal{V}(\mathcal{C}')\}. \quad (2)$$

Note that $\mathbf{T}_K^{(1)}$ can be determined by Φ, and thus it is a fiber process [29, p. 280] generated by Φ. Because Φ is stationary and isotropic, $\mathbf{T}_K^{(1)}$ is also stationary and isotropic.

2) Random Circumferences in DBC Mode: In the DBC mode, by symmetry, a user connects (resp. disconnects) with a BS if any only if it enters (resp. leaves) the disk region centered at the BS with a radius of R. Therefore, each BS generates a circumference (centered at the BS with a radius of R), and $\Xi_R^{(1)}$ is the union of all circumferences generated by all BSs. $\Xi_R^{(1)}$ is formally defined as follows:

$$\Xi_R^{(1)} = \bigcup_{\mathbf{x} \in \Phi} \mathcal{D}(\mathbf{x}, R). \quad (3)$$

where $\mathcal{D}(\mathbf{x}, r)$ is defined as the circumference $\{\mathbf{y} \in \mathbb{R}^2 \big| |\mathbf{x} - \mathbf{y}| = r\}$.

IV. Handoff Rate Analysis

In this section, we present an analytical framework to quantify the handoff rate. We first investigate the NBC mode by rewriting $\mathbf{T}_K^{(1)}$ in a more appropriate form. Then, the handoff rate is derived through analyzing the length intensity of $\mathbf{T}_K^{(1)}$, which is in turn derived through characterizing the area intensity of the Δd-neighborhood of $\mathbf{T}_K^{(1)}$. Finally, we derive the handoff rate in the DBC mode.

Note that in the rest of this paper, we define $\mathcal{B}(\mathbf{x}, r)$ as the disk region $\{\mathbf{y} \in \mathbb{R}^2 \big| |\mathbf{x} - \mathbf{y}| \leq r\}$, and $\mathcal{B}_c(\mathbf{x}, r)$ as the region $\{\mathbf{y} \in \mathbb{R}^2 \big| |\mathbf{x} - \mathbf{y}| \geq r\}$.

A. Rewriting Cell Boundary $\mathbf{T}_K^{(1)}$ in NBC Mode

We first rewrite $\mathbf{T}_K^{(1)}$ in a more appropriate form, which will facilitate the handoff analysis in the subsequent steps.

Theorem 1: $\mathbf{T}_K^{(1)}$ can be rewritten as follows:

$$\begin{aligned}\mathbf{T}_K^{(1)} = \{\mathbf{y} \in \mathbb{R}^2 | \exists \{\mathbf{x}_1, \mathbf{x}_2, \ldots, \mathbf{x}_{K-1}, \mathbf{x}_K, \mathbf{x}'_K\} \subset \Phi,\\ \text{s.t. } |\mathbf{z} - \mathbf{y}| \leq |\mathbf{x}_K - \mathbf{y}| = |\mathbf{x}'_K - \mathbf{y}| \leq |\mathbf{x} - \mathbf{y}|, \forall \mathbf{z} \in\\ \{\mathbf{x}_1, \ldots, \mathbf{x}_{K-1}\} \quad \text{and}\\ \forall \mathbf{x} \in \Phi \backslash \{\mathbf{x}_1, \ldots, \mathbf{x}_{K-1}, \mathbf{x}_K, \mathbf{x}'_K\}\}. \quad (4)\end{aligned}$$

See Appendix A for the proof.

Theorem 1 suggests that $\mathbf{T}_K^{(1)}$ is the set of points, whose distances to two BSs are the same, and this distance is greater than or equal to the distances to some arbitrary set of $K - 1$ BSs, but is less than or equal to the distances to all the other BSs.

B. Length Intensity and Area Intensity in NBC Mode

Handoffs occur at the intersections between an active user's trajectory with $\mathbf{T}_K^{(1)}$. In order to track the number of intersections, we need to first study the intensity of $\mathbf{T}_K^{(1)}$. Higher intensity of $\mathbf{T}_K^{(1)}$ leads to greater opportunities for boundary crossing, and thus higher handoff rate.

Let $\mu_1(\mathbf{T}_K^{(1)})$ denote the length intensity of $\mathbf{T}_K^{(1)}$, which is defined as the expected length of $\mathbf{T}_K^{(1)}$ in a unit square. Because $\mathbf{T}_K^{(1)}$ is stationary and isotropic, the unit square could be arbitrarily picked on $\mathbb{R}^2$. Hence, we have

$$\mu_1(\mathbf{T}_K^{(1)}) = \mathbb{E}\left(\left|\mathbf{T}_K^{(1)} \bigcap [0, 1)^2\right|_1\right), \quad (5)$$

where $|L|_1$ denotes the length of a collection of curves L (i.e., one-dimensional Lebesgue measure of L).

In order to derive $\mu_1(\mathbf{T}_K^{(1)})$, we need to introduce the Δd-extended cell boundary of $\mathbf{T}_K^{(1)}$, denoted by $\mathbf{T}_K^{(2)}(\Delta d)$, which is defined as

$$\mathbf{T}_K^{(2)}(\Delta d) = \left\{\mathbf{y} \in \mathbb{R}^2 \,\middle|\, \exists \mathbf{x} \in \mathbf{T}_K^{(1)}, \text{ s.t. } |\mathbf{x} - \mathbf{y}| < \Delta d\right\}. \quad (6)$$

In other words, $\mathbf{T}_K^{(2)}(\Delta d)$ is the Δd-neighborhood of $\mathbf{T}_K^{(1)}$. A point is in $\mathbf{T}_K^{(2)}(\Delta d)$ if and only if its (shortest) distance to $\mathbf{T}_K^{(1)}$ is less than Δd.

The area intensity of $\mathbf{T}_K^{(2)}(\Delta d)$ is defined as the expected area of $\mathbf{T}_K^{(2)}(\Delta d)$ in a unit square:

$$\mu_2(\mathbf{T}_K^{(2)}(\Delta d)) = \mathbb{E}\left(\left|\mathbf{T}_K^{(2)}(\Delta d) \bigcap [0, 1)^2\right|_2\right), \quad (7)$$

where $|S|_2$ denotes the area of some region S (i.e., two-dimensional Lebesgue measure of S).

Note that $\mathbf{T}_K^{(2)}(\Delta d)$ is stationary and isotropic. As a result, given a reference user located at $\mathbf{0}$, the area intensity of $\mathbf{T}_K^{(2)}(\Delta d)$ is equal to the probability that the reference user at $\mathbf{0}$ is in $\mathbf{T}_K^{(2)}(\Delta d)$.

$$\mu_2\big(\mathbf{T}_K^{(2)}(\Delta d)\big) = \mathbb{P}(\mathbf{0} \in \mathbf{T}_K^{(2)}(\Delta d)). \tag{8}$$

The probability in (8) is analytically tractable, which will be presented in the next subsection.

C. Derivations of Area Intensity of $\mathbf{T}_K^{(2)}(\Delta d)$ in NBC Mode

In this subsection, we present the derivation of $\mathbb{P}\left(\mathbf{0} \in \mathbf{T}_K^{(2)}(\Delta d)\right)$. First, we study the probability that the reference user at $\mathbf{0}$ is in $\mathbf{T}_K^{(2)}(\Delta d)$, given the distance between $\mathbf{0}$ and its Kth closest BS. We observe the following theorem:

Theorem 2: Suppose the reference user is located at $\mathbf{0}$, the distance between the reference user and its Kth closest BS is R_K. The conditional probability of $\mathbf{0} \in \mathbf{T}_K^{(2)}(\Delta d)$ given $R_K = r_0$ is

$$\mathbb{P}\left(\mathbf{0} \in \mathbf{T}_K^{(2)}(\Delta d) | R_K = r_0\right) = 8\lambda \Delta d r_0 + o(\Delta d^2). \tag{9}$$

See Appendix B for the proof.

Second, through deconditioning on R_K, we can derive the unconditioned probability that the reference user at $\mathbf{0}$ is in $\mathbf{T}_K^{(2)}(\Delta d)$.

Theorem 3: The area intensity of $\mathbf{T}_K^{(2)}(\Delta d)$ is

$$\begin{aligned}\mu_2\big(\mathbf{T}_K^{(2)}(\Delta d)\big) &= \mathbb{P}(\mathbf{0} \in \mathbf{T}_K^{(2)}(\Delta d)) \\ &= \frac{8\Gamma\left(\frac{1}{2}+K\right)\sqrt{\lambda}\Delta d}{\Gamma(K)\sqrt{\pi}} + o(\Delta d^2),\end{aligned} \tag{10}$$

where $\Gamma(\cdot)$ denotes the Gamma function.

See Appendix C for the proof.

D. From Area Intensity to Handoff Rate in NBC Mode

We first derive the length intensity of $\mathbf{T}_K^{(1)}$ from the area intensity of $\mathbf{T}_K^{(2)}(\Delta d)$:

$$\mu_1\big(\mathbf{T}_K^{(1)}\big) = \lim_{\Delta d \to 0} \frac{\mu_2\big(\mathbf{T}_K^{(2)}(\Delta d)\big)}{2\Delta d} \tag{11}$$

$$= \frac{4\Gamma\left(\frac{1}{2}+K\right)\sqrt{\lambda}}{\Gamma(K)\sqrt{\pi}}, \tag{12}$$

where (11) is obtained by noting the relationship between the total length of a collection of curves in $\mathbb{R}^2$ and the total area of their Δd-neighborhood [30, Sec. 3.2].

Second, we note that the expected number of intersections between an arbitrary curve and a stationary and isotropic fiber process in $\mathbb{R}^2$ is $\frac{2}{\pi}$ multiplied by both the length of the curve and the length intensity of the fiber process [29, Sec. 9.3]. Therefore, the expected number of intersections between an arbitrary user's trajectory $\mathcal{T}_0$ and $\mathbf{T}_K^{(1)}$ (i.e., handoffs) is given by

$$\mathbb{E}\left(\mathcal{N}(\mathcal{T}_0, \mathbf{T}_K^{(1)})\right) = \frac{2}{\pi}\mu_1\big(\mathbf{T}_K^{(1)}\big)|\mathcal{T}_0|_1, \tag{13}$$

where $|\mathcal{T}_0|_1$ denotes the length of $\mathcal{T}_0$.

Finally, let v denote the instantaneous speed of an active user, and $H(K, v)$ denote its handoff rate given K and v. Then, from (12)-(13) we have

$$H(K, v) = \frac{8\Gamma\left(\frac{1}{2}+K\right)\sqrt{\lambda}}{\Gamma(K)\pi\sqrt{\pi}} v. \tag{14}$$

E. One Useful Property of Handoffs in NBC Mode

Whenever a user makes a handoff, the user is at $\mathbf{T}_K^{(1)}$. From (4), we know that the distances from the user to two reference BSs are the same, and this reference distance is greater than or equal to the distances to some arbitrary set of $K-1$ BSs, but is less than or equal to the distances to all the other BSs. Since BSs are randomly distributed on the two-dimensional space, the probability that the reference distance is exactly equal to the distance between the user to any BSs other than the two reference BSs is 0. Thus, with probability 1, the handoff is made only between the two reference BSs, and none of the other BSs are involved. Therefore, we can conclude that with probability 1, a handoff is a soft handoff where only one of the K connected BSs is changed. In this case, (14) is equivalent to the soft handoff rate where only one of the K connected BSs is changed. Other types of handoff rates, where more than one BSs are changed, are all 0.

Note that the handoffs in the user-centric clustering scenario are quite different with those in the disjoint clustering scenario. In the disjoint clustering scenario, the entire cluster of BSs are changed when the user crosses the cluster boundary.

F. Handoff Analysis in DBC Mode

As seen in Section III-C2, each point of Φ generates a circumference with length $2\pi R$. Since there are λ points per unit area in expectation, the expected length of $\Xi_R^{(1)}$ in a unit area is $2\pi R\lambda$. We have

$$\mu_1\big(\Xi_R^{(1)}\big) = 2\pi R\lambda. \tag{15}$$

Let $H'(R, v)$ denote handoff rate given R and v. Similar to the derivations in (13) and (14), we have

$$H'(R, v) = 4R\lambda v. \tag{16}$$

Note that whenever a user makes a handoff, we know that the distance from the user to some reference BS is R. The probability that there is another BS at distance R from the user is 0. Thus, with probability 1, only one BS is connected or disconnected when a handoff occurs, and none of the other BSs are involved. This is different from the NBC case, where two BSs are involved in any handoff.

V. Downlink User Data Rate Analysis and Optimal BS Cluster Size

In this section, we present an application scenario of the above handoff rate analysis. In both the NBC and DBC modes, we study the downlink user data rate under the NC-JT scheme. Then, we discuss the optimal cluster size K that balances the handoff rate and the data rate. Note that we focus on the NC-JT scheme because it is one of the most commonly

adopted cooperative transmission schemes in practical systems [31], and it is easily implemented since the tight synchronization of joint signal transmission is not required [3].

Previous works such as [3] and [12] derived the downlink user data rate in non-closed form with multiple levels of integration, which brings great difficulty to design the optimal cluster size. In this work, we propose an alternative method, where a constant term with respect to the cluster size is ignored in the data rate analysis, and the optimal cluster size is then derived in a simplified way.

A. Non-Coherent Joint Transmission Model

In this subsection, we briefly present the channel model and the NC-JT scheme. In addition to the general user-centric model presented in Section III, we make additional assumptions as follows.

We assume that each user and BS is equipped with a single-antenna. Each BS transmits at power level P. If a BS is located at $\mathbf{x}$, then the received power at $\mathbf{y}$ is $\frac{Ph_{\mathbf{x},\mathbf{y}}}{|\mathbf{x}-\mathbf{y}|^{\alpha}}$, where $\alpha > 2$ is the pathloss exponent, $|\mathbf{x}-\mathbf{y}|^{\alpha}$ is the propagation loss function, and $h_{\mathbf{x},\mathbf{y}}$ is the normalized fast fading term. Corresponding to common Rayleigh fading with power normalization, $h_{\mathbf{x},\mathbf{y}}$ is independently exponentially distributed with unit mean. After assigning BSs to a user (either the K closest ones or the ones within a distance of R), NC-JT is implemented in the downlink transmission, so that the user receives a non-coherent sum of multiple copies of the useful signal transmitted by the cooperative BSs, and BSs not in the cooperation set generate interference to the user [3], [12]. In addition, we focus on the interference limited scenario, where the noise is negligible.

B. Data Rate in NBC Mode

1) Data Rate Analysis: In this subsection, we study the average user data rate via stochastic geometric analysis in the NBC mode. Due to the stationarity of BSs, we focus on the average performance of a reference user located at $\mathbf{0}$, which is equivalent to the average user performance in the system [26, p. 19].

Without loss of generality, we assume that the user is operated on a unit frequency bandwidth. Following the discussion in [3] and [12], under NC-JT, the signal-to-interference ratio (SIR) at the reference user is expressed as

$$\mathrm{SIR}(K) = \frac{\sum_{\mathbf{x}\in\Phi_K} |\mathbf{x}|^{-\alpha} h_{\mathbf{x},\mathbf{0}}}{\sum_{\mathbf{x}\in\Phi_K^c} |\mathbf{x}|^{-\alpha} h_{\mathbf{x},\mathbf{0}}}, \tag{17}$$

where Φ_K corresponds to the point process of the K (closest) cooperative BSs, and Φ_K^c corresponds to the point process of the other non-cooperative BSs. Let $S(K) \triangleq \sum_{\mathbf{x}\in\Phi_K} |\mathbf{x}|^{-\alpha} h_{\mathbf{x},\mathbf{0}}$ be the received signal power from the K cooperative BSs, and $I(K) \triangleq \sum_{\mathbf{x}\in\Phi_K^c} |\mathbf{x}|^{-\alpha} h_{\mathbf{x},\mathbf{0}}$ be the sum interference caused by non-cooperative BSs. Following conventional stochastic geometric analysis, we study the worst case scenario where the interference is summed over all non-cooperative BSs [2], [3], [12], [13]. Then, the average data rate of the reference user is

$$\begin{aligned} \mathrm{R}(K) &= \mathbb{E}\left[\log_2(1+\mathrm{SIR}(K))\right] \\ &= \mathbb{E}\left[\log_2(S(K)+I(K))\right] - \mathbb{E}\left[\log_2(I(K))\right]. \end{aligned} \tag{18}$$

Note that we have

$$S(K) + I(K) = \sum_{\mathbf{x}\in\Phi} |\mathbf{x}|^{-\alpha} h_{\mathbf{x},\mathbf{0}}, \tag{19}$$

which is a term irrelevant to K. Since we aim to derive the optimal K, the term $\mathbb{E}\left[\log_2(S(K)+I(K))\right] \triangleq C_0$ can be regarded as a constant and is ignored in the subsequent analysis.

In the next step, we study $\mathbb{E}\left[\log_2(I(K))\right]$. However, this term is still difficult to characterize. Therefore, we resort to analyzing its upper bound using Jensen's inequality:

$$\mathbb{E}\left[\log_2(I(K))\right] \le \log_2(\mathbb{E}[I(K)]). \tag{20}$$

Correspondingly, we focus on a lower bound of the average data rate as follows:

$$\widetilde{\mathrm{R}}(K) = C_0 - \log_2(\mathbb{E}[I(K)]). \tag{21}$$

As shown in Sections V-B2 and V-C, the characterization of $\log_2(\mathbb{E}[I(K)])$ instead of $\mathbb{E}\left[\log_2(I(K))\right]$ will lead to a simple closed-form expression, which can then be used to search for the optimal K in a simplified manner. As shown in Section VI, the values of $\mathbb{E}\left[\log_2(I(K))\right]$ are close to those of $\log_2(\mathbb{E}[I(K)])$ over a wide range of parameter settings. Therefore, the approximation of $\mathbb{E}\left[\log_2(I(K))\right]$ by $\log_2(\mathbb{E}[I(K)])$ is an important simplification step in deriving the optimal K.

We note that the analytical steps from (18) to (21) differentiate our work with those in the existing literature, such as [3] and [12], where the user data rate is expressed in non-closed form with multiple levels of integration due to difficulties arising from the PPP generating functional. Since our aim is to find the optimal cluster K in closed form, we require a closed form expression for the data rate. For the data rate expression in (21), we will show next how to derive $\log_2(\mathbb{E}[I(K)])$ in closed form. Even though C_0 has not been explicitly derived, it is a constant under all K values and thus can be omitted in the subsequent optimization of K.

2) Derivation of $\mathbb{E}[I(K)]$: The overall interference is summed over all BSs outside the set of K closest BSs to $\mathbf{0}$. Given the distance from the reference user to its Kth closest BS $R_K = r_0$, the point process of Φ_K^c is a PPP with intensity λ in the range $\mathcal{B}_c(\mathbf{0}, r_0)$. Therefore, the conditional average interference can be computed as

$$\mathbb{E}[I(K)|R_K = r_0] = \lambda \int_{\mathcal{B}_c(\mathbf{0},r_0)} |\mathbf{x}|^{-\alpha} \mathrm{d}\mathbf{x} \tag{22}$$

$$= 2\pi\lambda \int_{r_0}^{\infty} r^{1-\alpha} \mathrm{d}r = 2\pi\lambda \frac{r_0^{2-\alpha}}{\alpha-2}. \tag{23}$$

Then, through deconditioning on R_K, and considering (23) and (44), we have

$$\mathbb{E}[I(K)] = \int_0^{\infty} 2\pi\lambda \frac{r_0^{2-\alpha}}{\alpha-2} \frac{2(\lambda\pi r_0^2)^K}{r_0\Gamma(K)} \exp(-\lambda\pi r_0^2) \mathrm{d}r_0 \tag{24}$$

$$= \frac{2\pi^{\frac{\alpha}{2}} \lambda^{\frac{\alpha}{2}} \Gamma(K+1-\frac{\alpha}{2})}{(\alpha-2)\Gamma(K)}. \tag{25}$$

Finally, the term $\log_2(\mathbb{E}[I(K)])$ can be derived accordingly from (25).

C. Optimal Cluster Size in NBC Mode

In this subsection, we investigate the optimal cluster size based on the handoff rate study in Section IV and the data rate study in Sections V-B1 and V-B2. Let K^* denote the optimal cluster size. K^* is an integer greater than or equal to $K_{\min}$.

In order to quantify the tradeoff between user data rate and handoff cost, we consider their weighted sum. Let W_1 be the utility value for one bit of data transmission, and W_2 be the cost for one handoff. Note that W_2 is a general cost that covers many factors, such as signaling overhead of a handoff and the penalty of potential handoff failure due to random system errors. We assign the same cost value to all handoffs because each of them is a soft handoff where only one of the K connected BSs is changed with probability 1, as shown in Section IV-E. Consequently, the overall average utility of a user being served by K BSs is

$$\begin{aligned} U(K) &= W_1\widetilde{\mathrm{R}}(K) - W_2 H(K) = W_1 C_0 \\ &\quad - W_1 \log_2(e) \ln\left(\frac{2\pi^{\frac{\alpha}{2}}\lambda^{\frac{\alpha}{2}}\Gamma(K+1-\frac{\alpha}{2})}{(\alpha-2)\Gamma(K)}\right) \\ &\quad - W_2 \frac{8\Gamma\left(\frac{1}{2}+K\right)\sqrt{\lambda}}{\Gamma(K)\pi\sqrt{\pi}}\upsilon. \end{aligned} \tag{26}$$

We define $L(K) \triangleq \ln\left(\frac{2\pi^{\frac{\alpha}{2}}\lambda^{\frac{\alpha}{2}}\Gamma(K+1-\frac{\alpha}{2})}{(\alpha-2)\Gamma(K)}\right)$ and $H(K) \triangleq \frac{8\Gamma\left(\frac{1}{2}+K\right)\sqrt{\lambda}}{\Gamma(K)\pi\sqrt{\pi}}\upsilon$. K^* is the integer that maximizes $U(K)$, or equivalently, minimizes $W_1\log_2(e)L(K) + W_2\, H(K)$.

We also define

$$\begin{aligned} \Delta H(K) &\triangleq H(K+1) - H(K) \\ &= W_2 \frac{\Gamma(K+\frac{1}{2})}{\Gamma(K+1)}\frac{1}{2}\frac{8\sqrt{\lambda}}{\pi\sqrt{\pi}}\upsilon, \end{aligned} \tag{27}$$

and

$$\begin{aligned} \Delta L(K) &\triangleq L(K+1) - L(K) \\ &= W_1 \log_2(e) \ln\left(\frac{K+1-\frac{\alpha}{2}}{K}\right). \end{aligned} \tag{28}$$

It is straightforward to show that $\Delta H(K)$ is positive and $\Delta L(K)$ is negative, so that $H(K)$ is an increasing function and $L(K)$ is a decreasing function. In the next step, in order to derive the optimal K^*, we focus on the term $-\frac{\Delta H(K)}{\Delta L(K)}$. We note that $-\frac{\Delta H(K)}{\Delta L(K)} < 1$ implies that $H(K)+L(K)$ is decreasing at K and $-\frac{\Delta H(K)}{\Delta L(K)} > 1$ implies that $H(K)+L(K)$ is increasing at K. Also, we have the following theorem:

Theorem 4: $-\frac{\Delta H(K)}{\Delta L(K)}$ is an increasing function of K.

See Appendix D for the proof.

In addition to Theorem 4, we notice that $-\frac{\Delta H(K)}{\Delta L(K)} \to \infty$ when K is sufficient large, and $-\frac{\Delta H(K)}{\Delta L(K)} \to 0$ when K approaches $\frac{\alpha}{2}-1$. Let $\widetilde{K}^*$ be the solution to $-\frac{\Delta H(K)}{\Delta L(K)} = 1$, then we have the following conclusion:

- If $-\frac{\Delta H(K_{\min})}{\Delta L(K_{\min})} \geq 1$, then $H(K)+L(K)$ is an increasing function and $K^* = K_{\min}$.
- Otherwise, $H(K)+L(K)$ is firstly decreasing and then increasing, and K^* is equal to $\lfloor\widetilde{K}^*\rfloor$ or $\lceil\widetilde{K}^*\rceil$, whichever that minimizes $H(K)+L(K)$.

1) Asymptotic Value of $\widetilde{K}^*$: From the previous subsection, we see that $\widetilde{K}^*$ is the solution to $-\frac{\Delta H(K)}{\Delta L(K)} = 1$, which can be derived through a simple numerical search. However, it is not in closed form. For deeper insights in characterizing K^*, We are interested in further seeking an approximated expression of $\widetilde{K}^*$ in closed form.

First, we observe the asymptotic values of $\Delta L(K)$ and $\Delta H(K)$, when K is large, are:

$$\Delta L(K) \simeq -W_1 \log_2(e)\frac{\left(\frac{\alpha}{2}-1\right)}{K}, \tag{29}$$

and

$$\Delta H(K) \simeq \frac{W_2}{\sqrt{K}}\frac{4\sqrt{\lambda}}{\pi\sqrt{\pi}}\upsilon. \tag{30}$$

Then, by substituting the right-hand sides of (29) and (30) into $-\frac{\Delta H(K)}{\Delta L(K)} = 1$, we derive the asymptotic value of $\widetilde{K}^*$, denoted by $\widehat{K}^*$, as follows:

$$\widehat{K}^* = \frac{W_1^2\left(\log_2(e)\right)^2\left(\frac{\alpha}{2}-1\right)^2\pi^3}{16W_2^2\lambda\upsilon^2}. \tag{31}$$

The expression (31) suggests that the optimal cluster size is asymptotically inversely proportional to the square of the user speed υ and asymptotically inversely proportional to the BS intensity λ. Note that in Section VI, we further show through numerical study that even if $\widetilde{K}^*$ is not large, the values of $\widehat{K}^*$ are still close to those of $\widetilde{K}^*$.

In summary, we reach the following corollary:

Corollary 1: In the NBC mode, the optimal cluster size is asymptotically inversely proportional to the square of the user speed υ and asymptotically inversely proportional to the BS intensity λ.

D. Data Rate and Optimal Cluster Size in DBC Mode

In this subsection, we study the data rate and the optimal cluster size in the DBC mode. First, given R, the SIR at a reference user located at $\mathbf{0}$ is expressed as

$$\mathrm{SIR}'(R) = \frac{\sum_{\mathbf{x}\in\Phi_R}|\mathbf{x}|^{-\alpha}h_{\mathbf{x},\mathbf{0}}}{\sum_{\mathbf{x}\in\Phi_R^c}|\mathbf{x}|^{-\alpha}h_{\mathbf{x},\mathbf{0}}}, \tag{32}$$

where Φ_R corresponds to the point process of the cooperative BSs within a distance of R from the reference user, and Φ_R^c corresponds to the point process of non-cooperative BSs. Let $S'(R) \triangleq \sum_{\mathbf{x}\in\Phi_R}|\mathbf{x}|^{-\alpha}h_{\mathbf{x},\mathbf{0}}$ be the received signal power from the cooperative BSs, and $I'(R) \triangleq \sum_{\mathbf{x}\in\Phi_R^c}|\mathbf{x}|^{-\alpha}h_{\mathbf{x},\mathbf{0}}$ be the sum interference caused by non-cooperative BSs. We aim to study the average data rate

$$\mathrm{R}'(K) = \mathbb{E}\left[\log_2(1+\mathrm{SIR}'(K))\right]. \tag{33}$$

We have

$$S'(R) + I'(R) = \sum_{\mathbf{x}\in\Phi}|\mathbf{x}|^{-\alpha}h_{\mathbf{x},\mathbf{0}}, \tag{34}$$

which is a term irrelevant to R. Therefore, similar to (18)–(21), we focus on a lower bound of the average data rate as follows:

$$\widetilde{\mathrm{R}}'(R) = C_0 - \log_2(\mathbb{E}[I'(R)]), \tag{35}$$

where $\mathbb{E}[I'(R)]$ can be derived as follows:

$$\mathbb{E}[I'(R)] = \lambda \int_{\mathcal{B}_c(\mathbf{0},R)} |\mathbf{x}|^{-\alpha} \mathrm{d}\mathbf{x} \tag{36}$$

$$= 2\pi\lambda \int_R^\infty r^{1-\alpha} \mathrm{d}r = 2\pi\lambda \frac{R^{2-\alpha}}{\alpha - 2}. \tag{37}$$

Similar to Section V-C, we study the weighted sum of data rate and handoff rate. Recall that W_1 is the utility value for one bit of data transmission. We further define W_2' as the cost for one handoff in the DBC mode. Consequently, the overall average utility of a user under R is

$$\begin{aligned} U'(R) &= W_1 \widetilde{\mathrm{R}}'(R) - W_2' H(R) \\ &= W_1 C_0 - W_1 \log_2(e) \ln\left(2\pi\lambda \frac{R^{2-\alpha}}{\alpha - 2}\right) - W_2' 4R\lambda v. \end{aligned} \tag{38}$$

By taking the first order derivative, we can show that (38) is minimized when R is

$$R^* = \frac{W_1 \log_2(e)(\alpha - 2)}{4W_2'\lambda v}. \tag{39}$$

Therefore, the optimal cluster size is

$$\overline{K}^* = \pi (R^*)^2 \lambda = \frac{W_1^2 \left(\log_2(e)\right)^2 (\alpha - 2)^2 \pi}{16 (W_2')^2 \lambda v^2}. \tag{40}$$

We observe that the optimal cluster size is inversely proportional to the square of the user speed v and inversely proportional to the BS intensity λ.

In summary, we reach the following corollary:

Corollary 2: In the DBC mode, the optimal cluster size is inversely proportional to the square of the user speed v and inversely proportional to the BS intensity λ.

VI. Simulation Study

In this section, we present simulation studies to validate the accuracy and usefulness of our proposed analysis. In each round of simulation, BSs are generated on a 20 km × 20 km square. Then, we randomly generate 5 waypoints $\mathbf{X}_1, \mathbf{X}_2, \ldots, \mathbf{X}_5$ in the central 10 km × 10 km square. The four line segments $\mathbf{X}_1\mathbf{X}_2, \mathbf{X}_2\mathbf{X}_3, \ldots, \mathbf{X}_4\mathbf{X}_5$ form the trajectory of an active user in one round of simulation. By tracking which set of BSs the user is connected to along its trajectory, we can track handoffs of the user in this round of simulation. Each data point is averaged over 2000 simulation rounds.

A. Simulation on Handoff Rate

We first study the handoff rates under different K and λ values in Figs. 4 and 5. The BS intensity is set to $\lambda = 1$, 2, 3, and 4 units/km^2 respectively, and the user speed is $v = 20$ km/h. As discussed in Section III-A, we are also interested in testing the scenario where BSs are non-PPP distributed. Thus in the simulation, we also consider the case where BSs are distributed as a Matérn hard core (MHC) point process.

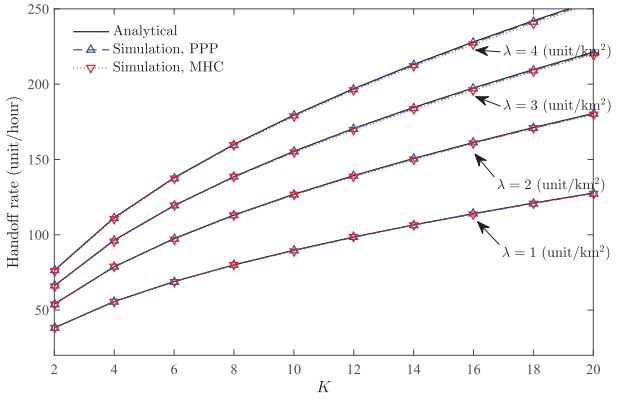

Fig. 4. NBC mode. Handoff rate under different K.

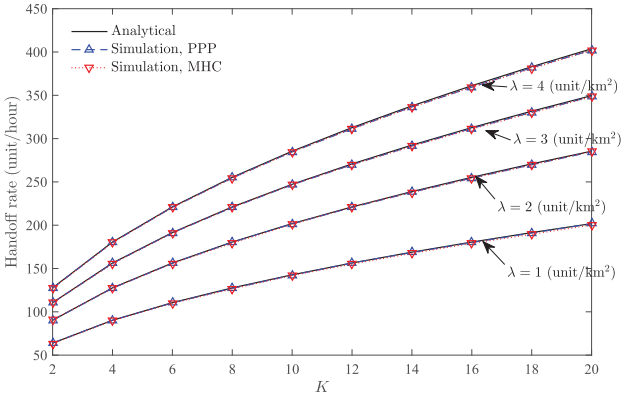

Fig. 5. DBC mode. Handoff rate under different K.

PPP does not perfectly match the distributions of BSs in reality [32], [33]. The issue mainly stems from the strong Markov property of PPP [26, p. 17]: The distribution of points in one region is independent of the distribution of points in another region as long as these two regions are non-overlapping. However, in practice, the network operator does not install BSs in close proximity to each other. The MHC point process is an alternative to counter the drawback of PPP modeling [32], [33]. In particular, it avoids the possibility that two BSs are located arbitrarily close to each other. Specifically, BSs are generated as an MHC point process as follows [26, p. 26]:

1) We generate a PPP with intensity λ'.
2) Each point in the PPP is associated with a "mark", which is independently uniformly distributed on [0, 1].
3) Each point is retained or removed according to the following rule:
   - If the point's mark is the largest among all the points within a distance D from it (or there is no other point within a distance D from it), the point is retained.
   - Otherwise, the point it is removed.
4) All retained points form the MHC point process.

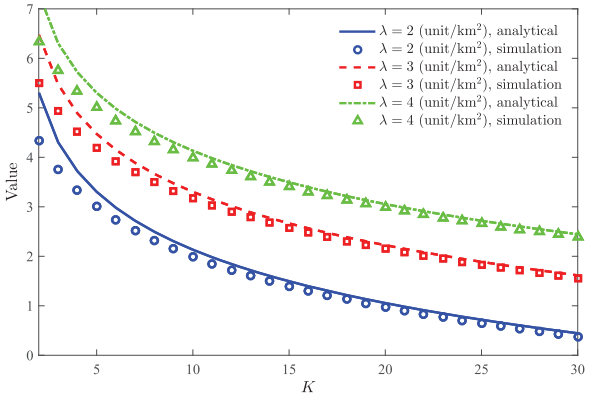

Fig. 6. NBC mode. Comparison of simulated $\mathbb{E}\left[\log_2(I(K))\right]$ and analytical $\log_2(\mathbb{E}[I(K)])$.

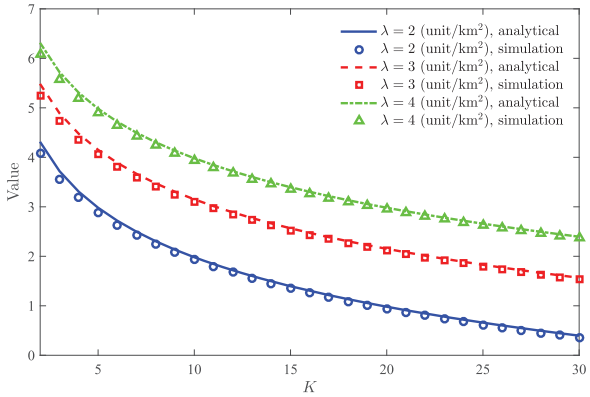

Fig. 7. DBC mode. Comparison of simulated $\mathbb{E}\left[\log_2(I'(K))\right]$ and analytical $\log_2(\mathbb{E}[I'(K)])$.

Note that if a point is retained in the MHC point process, according to Step 3), there is no other retained point within a distance D from it. Therefore, the distance between any two points in the MHC point process is no less than D.

The equivalent BS intensity (intensity of retained points) of above generated MHC point process is $\lambda = \frac{1-e^{-\pi D^2\lambda'}}{\pi D^2}$. In this subsection, we set $D = 0.1$ km, $\lambda' = 1.0160$, 2.0656, 3.1509, and 4.2746 units/km^2 respectively, in order to maintain the equivalent BS intensity at $\lambda = 1$, 2, 3, and 4 units/km^2 respectively.

In the NBC mode, Fig. 4 validates that the handoff rate is an increasing and concave function of K, which matches the expression (14). Also, when the BSs are PPP distributed, the handoff rates obtained from simulation match well with our proposed analysis, validating the correctness of our analytical derivations in Section IV. Furthermore, even if the BSs are distributed as an MHC point process, the simulated handoff rates are still very close to those under the PPP assumption. Therefore, our proposed analysis is still useful to provide close approximations of handoff rates when BSs are more realistically distributed. In the DBC mode, Fig. 5 shows that the analytical handoff rates match well with simulated handoff rates under both PPP and MHC distributed BSs.

B. Simulation on Interference

In Fig. 6, we show a comparison between the values of $\mathbb{E}\left[\log_2(I(K))\right]$ through simulation and those of $\log_2(\mathbb{E}[I(K)])$ derived in Sections V-B1 and V-B2 in the NBC mode. Fig. 6 shows that the gap between $\mathbb{E}\left[\log_2(I(K))\right]$ and $\log_2(\mathbb{E}[I(K)])$ is small, so that we can use $\log_2(\mathbb{E}[I(K)])$ to approximate $\mathbb{E}\left[\log_2(I(K))\right]$ in the NBC mode. Similarly, in Fig. 7, we show a comparison between $\mathbb{E}\left[\log_2(I'(K))\right]$ through simulation and $\log_2(\mathbb{E}[I'(K)])$ derived in Sections V-D in the DBC mode,[3] which again suggests that the gaps between the two terms are small. Furthermore, under the same K, $\mathbb{E}\left[\log_2(I(K))\right]$ is greater than $\mathbb{E}\left[\log_2(I'(K))\right]$, and thus the average data rate in the NBC mode is lower than that in the DBC mode (see (21) and (35)).

[3]Note that in the DBC mode, there is a one-to-one mapping between K and R, and $I'(K)$ represents the sum interference caused by non-cooperative BSs when $K = \pi R^2\lambda$.

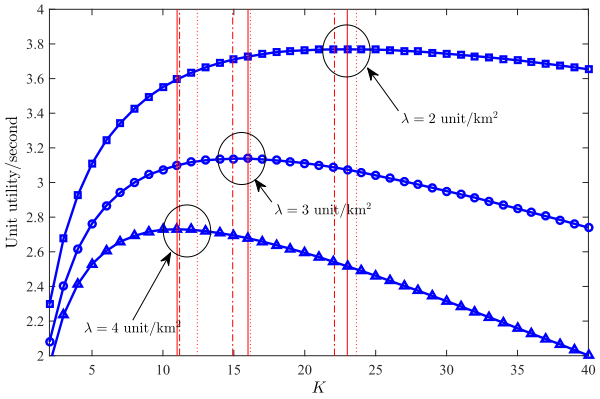

Fig. 8. NBC mode. User utility under different K. The solid, dotted, and dashed dotted vertical lines correspond to the optimal K^* derived by simulation, the analytical values of $\widetilde{K}^*$ and $\widehat{K}^*$ respectively.

C. Optimal Cluster Size

In Figs. 8–13, we study the weighted sum user utility and the optimal cluster size. As explained in Sections IV-E and IV-F, only one BS is connected or disconnected when a handoff occurs in the DBC mode, while two BSs are involved (one is connected and the other is disconnected) when a handoff occurs in the NBC mode. To properly compare these two modes, we set the cost of one handoff in the DBC mode half of the cost of one handoff in the NBC mode (i.e., $W_2' = \frac{1}{2}W_2$).

In Fig. 8, we present the simulated user utility $W_1\mathrm{R}(K) - W_2H(K)$ in the NBC mode under different values of the cluster size K. The network parameters are as follows: $\alpha = 4$, $W_1 = 1$, $W_2 = 30$, $v = 36$ km/h, and $P = 30$ dBm. The simulated results are plotted for $\lambda = 2$, 3, and 4 unit/km^2 respectively. The results validate that the simulated optimal solutions are close to $\widetilde{K}^*$, illustrating the effectiveness of our analysis in Section V. In addition, the asymptotically optimal solutions $\widehat{K}^*$ are also close to both the simulated optimal solutions and $\widetilde{K}^*$ values, illustrating the usefulness of the expression (31) even if the cluster size is not large. In Fig. 9, we present the simulated user utility $W_1\mathrm{R}'(K) - W_2'H'(K)$ in

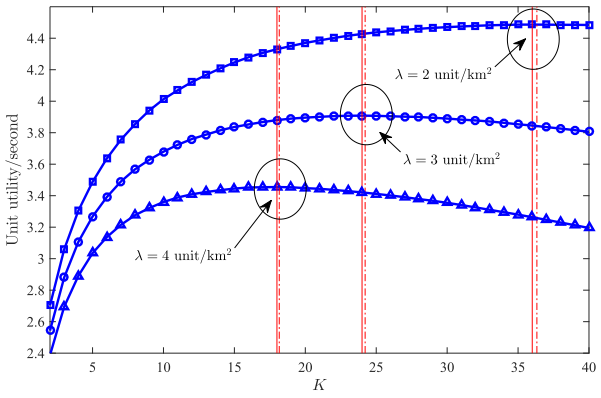

Fig. 9. DBC mode. User utility under different K. The solid and dashed dotted vertical lines correspond to the optimal K^* derived by simulation and the analytical values of $\overline{K}^*$ respectively.

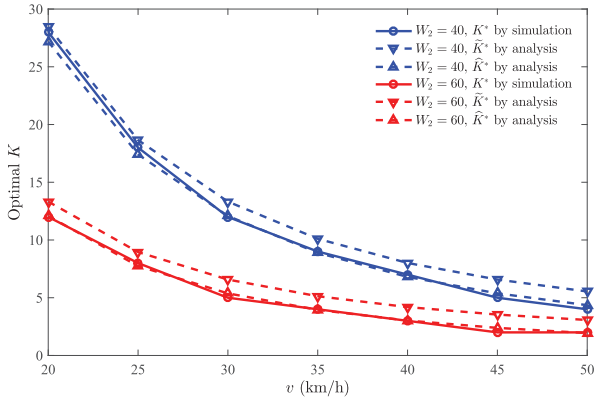

Fig. 10. NBC mode. Optimal K under different user speed v.

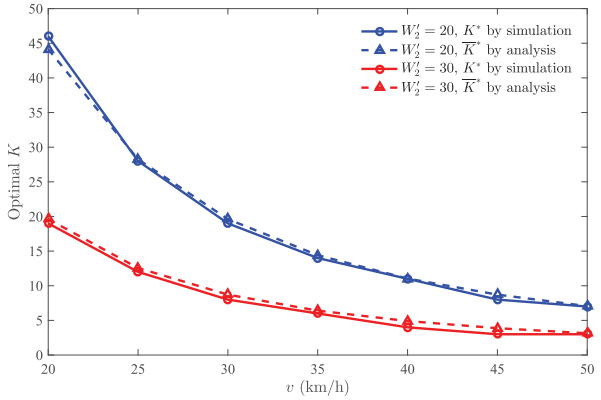

Fig. 11. DBC mode. Optimal K under different user speed v.

the DBC mode under different values of the cluster size K. All parameters are the same as those used in Fig. 8 except $W_2' = 15$. K^* represents the simulated optimal integer cluster size. The simulated optimal solutions are close to $\overline{K}^*$, illustrating the accuracy of expression (40).

In Figs. 10 and 11, we study the optimal cluster size K under different user speed v in the NBC and DBC modes, and in Figs. 12 and 13, we study the optimal K under different BS intensity λ in the NBC and DBC modes. In these figures,

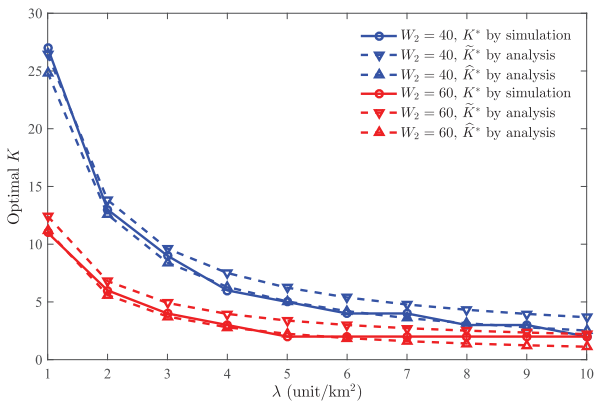

Fig. 12. NBC mode. Optimal K under different BS intensity λ.

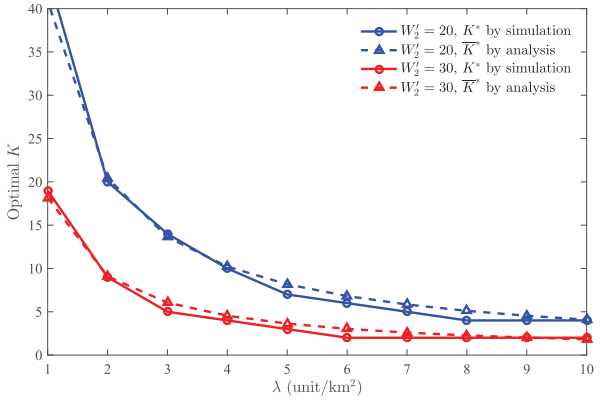

Fig. 13. DBC mode. Optimal K under different BS intensity λ.

we set $\alpha = 4$, $W_1 = 1$, and $P = 30$ dBm. In Figs. 10 and 11, we additionally set $\lambda = 3$ unit/km^2, and in Figs. 12 and 13, we additionally set $v = 36$ km/h.

In the NBC mode, both the analytical values of $\widetilde{K}^*$ and $\widehat{K}^*$ are close to the simulated optimal K^* under a wide range of user speeds and BS intensities. In addition, since the values of $\widehat{K}^*$ derived in (31) are close to the simulated results, it suggests that the optimal cluster size is approximately inversely proportional to the square of the user speed v and inversely proportional to the BS intensity λ even if K is not large. In the DBC mode, the analytical values of $\overline{K}^*$ are close to the simulated optimal K^* under a wide range of user speeds and BS intensities. Similar scaling behavior is observed: K^* is inversely proportional to v^2 and inversely proportional to λ.

We further observe from Figs. 6–9 that under the same K, the average data rate in the NBC mode is lower than that in the DBC mode, and the average handoff cost in the NBC mode is greater than that in the DBC mode. Therefore, under the same cluster size K, the DBC mode gives higher overall utility, although the NBC mode is easier to implement in practice. Hence, as shown in Figs. 10–13, the optimal cluster size in the DBC mode is greater than that in the NBC mode.

D. Networks With Limited Radio Resource

So far, our analyses and simulation results are based on the assumption that BSs have enough radio resource to serve the users. In what follows, we further consider a more practical

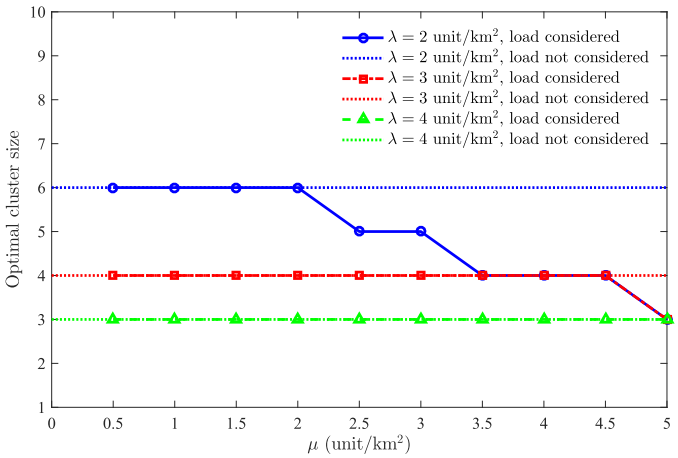

Fig. 14. Impact of limited radio resource on the optimal cluster size in the NBC mode.

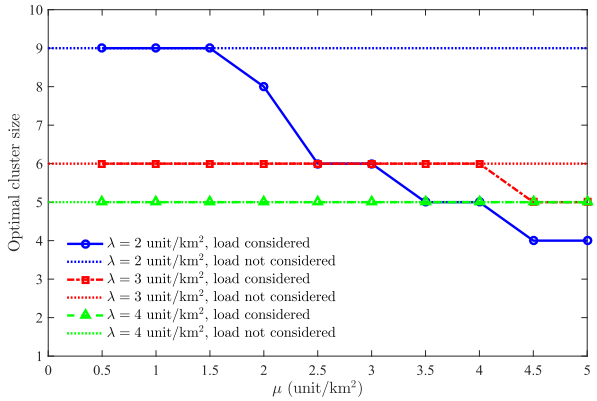

Fig. 15. Impact of limited radio resource on the optimal cluster size in the DBC mode.

scenario where BSs have limited radio resource and there are many users in the system. Note that in this scenario, our handoff rate analysis in Section IV is still accurate. This is because a handoff occurs whenever a user crosses the virtual cell boundary. However, our data rate analysis in Section V will be influenced. This is because some cooperative BSs may not have sufficient radio resource to serve their connected users. Moreover, a handoff may be unsuccessful if the new BSs do not have any resource to serve the user.

We assume that the system has 20 orthogonal radio resource blocks (RBs). Whenever a user enters the system or is handed off to a new virtual cell, it requests to be served by its cooperative N BSs (where N equals K in the NBC mode, or the number of BSs within a distance R in the DBC mode). The system looks for an RB that is commonly available at all of these N BSs. If such an RB can be found, the user is cooperatively served by these N BSs on the RB. Otherwise, the system looks for an RB that is available at $(N-1)$ of the BSs. If no RB is found again, the system looks for an RB that is available at $(N-2)$ BSs and so on. If the user cannot find even one available RB at one BS, the user is disconnected and its data rate is zero. In this scenario, the handoff is unsuccessful since the new BSs do not have any RBs to serve the user. The user's data rate remains zero until an RB becomes available again and thus the user can reconnect to the system. The other network parameters are as follows: $\alpha = 4$, $v = 36$ km/h, and $P = 30$ dBm. The density of users μ ranges from 0.5 to 5 units/km^2. We set $W_2 = 60$ in the NBC mode and $W_2' = 30$ in the DBC mode.

In Figs. 14 and 15, we show the optimal cluster size when we increase the user density. For reference, we also show the optimal cluster size derived in Section VI-C (when the user load is not considered). The results suggest that in both NBC and DBC, our analysis is accurate when the network is lightly loaded. However, when the network is more congested,[4] the optimal cluster size is smaller than our analytical estimation. This is because if we increase the cluster size K, more BSs should use their RBs to serve one user. Thus, it is more likely that some BSs do not have enough RBs to serve their connected users. As a consequence, a greater penalty in terms of data rate performance is incurred. The optimal cluster size depends on both the handoff rate and data rate. The handoff rate follows our analysis, but the data rate is penalized more and more as we increase K, so that the optimal K is smaller than our analytical estimation.

VII. Conclusion

In this work, we provide a theoretical framework to study the handoffs in cooperative wireless networks. We study two user-centric clustering modes, namely the number-based cooperation (NBC) mode and the distance-based cooperation (DBC) mode. Through our proposed stochastic geometric analysis, we capture the irregularly shaped network topology introduced by randomly distributed BSs and user-centric cooperation. In both modes, The analytical expression for the handoff rate experienced by an active user with arbitrary movement trajectory is derived. Based on this result, we also propose an optimal cluster size formulation considering both the handoff rate and the data rate. We observe that when the common NC-JT scheme is employed, in the NBC (resp. DBC) mode, the optimal cluster size is asymptotically inversely (resp. inversely) proportional to the square of the user speed and asymptotically inversely (resp. inversely) proportional to the BS intensity. Computer simulation is conducted, validating the correctness and usefulness of our analytical results. We further conclude that under the same cluster size, the DBC mode gives higher overall utility, and the optimal cluster size in the DBC mode is greater than that in the NBC mode.

Appendix

A. Proof of Theorem 1

Proof: For simplicity, we define $\mathbf{T}_K^{(1)'}$ as the right-hand side of (4). We show that $\mathbf{T}_K^{(1)'}$ and $\mathbf{T}_K^{(1)}$ are equivalent through the following two steps:

Step 1: $\mathbf{y} \in \mathbf{T}_K^{(1)'} \Rightarrow \mathbf{y} \in \mathbf{T}_K^{(1)}$.

Suppose $\mathbf{y} \in \mathbf{T}_K^{(1)'}$, then $\exists\{\mathbf{x}_1, \mathbf{x}_2, \ldots, \mathbf{x}_{K-1}, \mathbf{x}_K, \mathbf{x}_K'\}$, such that $|\mathbf{z}-\mathbf{y}| \leq |\mathbf{x}_K - \mathbf{y}| = |\mathbf{x}_K' - \mathbf{y}| \leq |\mathbf{x}-\mathbf{y}|, \forall \mathbf{z} \in \{\mathbf{x}_1, \mathbf{x}_2, \ldots, \mathbf{x}_{K-1}\}$ and $\forall \mathbf{x} \in \Phi \backslash \{\mathbf{x}_1, \ldots, \mathbf{x}_{K-1}, \mathbf{x}_K, \mathbf{x}_K'\}$. Let $\mathcal{C}_1 = \{\mathbf{x}_1, \ldots, \mathbf{x}_{K-1}, \mathbf{x}_K\}$, and $\mathcal{C}_2 = \{\mathbf{x}_1, \ldots, \mathbf{x}_{K-1}, \mathbf{x}_K'\}$. Following the definition in (1), we have $\mathbf{y} \in \mathcal{V}(\mathcal{C}_1)$ and

[4]Both increasing μ and decreasing λ will cause a more congested network.

$\mathbf{y} \in \mathcal{V}(\mathcal{C}_2)$. Therefore, by the definition of $\mathbf{T}_K^{(1)}$ in (3), $\mathbf{y}$ is at the boundary of $\mathcal{V}(\mathcal{C}_1)$ and $\mathcal{V}(\mathcal{C}_2)$ and thus $\mathbf{y} \in \mathbf{T}_K^{(1)}$.

Step 2: $\mathbf{y} \in \mathbf{T}_K^{(1)} \Rightarrow \mathbf{y} \in \mathbf{T}_K^{(1)'}$.

Suppose $\mathbf{y} \in \mathbf{T}_K^{(1)}$. First, following the definition in (3), $\exists \mathcal{C}_1'$ and $\mathcal{C}_2'$, such that $\mathbf{y} \in \mathcal{V}(\mathcal{C}_1')$ and $\mathbf{y} \in \mathcal{V}(\mathcal{C}_2')$. Let $\mathcal{C}_1' = \{\mathbf{z}_1, \mathbf{z}_2, \ldots, \mathbf{z}_n, \mathbf{u}_{n+1}, \ldots, \mathbf{u}_K\}$, and $\mathcal{C}_2' = \{\mathbf{z}_1, \mathbf{z}_2, \ldots, \mathbf{z}_n, \mathbf{v}_{n+1}, \ldots, \mathbf{v}_K\}$, where $\mathbf{z}_1, \mathbf{z}_2, \ldots, \mathbf{z}_n$ are the common elements in $\mathcal{C}_1'$ and $\mathcal{C}_2'$. Note that at least one element in $\mathcal{C}_1'$ is different from that in $\mathcal{C}_2'$, thus $n < K$.

In the second step, we compare the distances between $|\mathbf{u}_i - \mathbf{y}|$ and $|\mathbf{v}_j - \mathbf{y}|$, $\forall i, j \in \{n+1, n+2, \ldots, K\}$. Since $\mathbf{y} \in \mathcal{V}(\mathcal{C}_1')$, $\mathbf{u}_i \in \mathcal{C}_1'$ and $\mathbf{v}_j \notin \mathcal{C}_1'$, we have $|\mathbf{u}_i - \mathbf{y}| \leq |\mathbf{v}_j - \mathbf{y}|$ according to the definition of $\mathcal{V}(\mathcal{C}_1')$ in (1). Similarly, since $\mathbf{y} \in \mathcal{V}(\mathcal{C}_2')$, $\mathbf{v}_j \in \mathcal{C}_2'$ and $\mathbf{u}_i \notin \mathcal{C}_2'$, we have $|\mathbf{v}_j - \mathbf{y}| \leq |\mathbf{u}_i - \mathbf{y}|$. Therefore, we can conclude that $|\mathbf{v}_j - \mathbf{y}| = |\mathbf{u}_i - \mathbf{y}|$, $\forall i, j \in \{n+1, n+2, \ldots, K\}$. Finally, we have $|\mathbf{z}_k - \mathbf{y}| \leq |\mathbf{v}_j - \mathbf{y}| = |\mathbf{u}_i - \mathbf{y}| \leq |\mathbf{x} - \mathbf{y}|$, $\forall k \in \{1, 2, \ldots, n\}$, $\forall i, j \in \{n+1, n+2, \ldots, K\}$, and $\forall \mathbf{x} \in \Phi \backslash (\mathcal{C}_1' \bigcup \mathcal{C}_2')$.

Let $\mathbf{x}_1 = \mathbf{z}_1, \mathbf{x}_2 = \mathbf{z}_2, \ldots, \mathbf{x}_n = \mathbf{z}_n, \mathbf{x}_{n+1} = \mathbf{u}_{n+1}, \ldots, \mathbf{x}_K = \mathbf{u}_K, \mathbf{x}_K' = \mathbf{v}_K$, then we have $|\mathbf{z} - \mathbf{y}| \leq |\mathbf{x}_K - \mathbf{y}| = |\mathbf{x}_K' - \mathbf{y}| \leq |\mathbf{x} - \mathbf{y}|, \forall \mathbf{z} \in \{\mathbf{x}_1, \mathbf{x}_2, \ldots, \mathbf{x}_{K-1}\}$ and $\forall \mathbf{x} \in \Phi \backslash \{\mathbf{x}_1, \ldots, \mathbf{x}_{K-1}, \mathbf{x}_K, \mathbf{x}_K'\}$. Therefore, we have proved that $\mathbf{y} \in \mathbf{T}_K^{(1)'}$. □

B. Proof of Theorem 2

Proof: Without loss of generality, we assume the Kth closest BS is located at $\mathbf{x}_K = (r_0, 0)$. Note that there are no BSs other than the K BSs located within $\mathcal{B}(\mathbf{0}, r_0)$, where $\mathcal{B}(\mathbf{0}, r_0)$ is defined at the beginning of Section IV.

Following Theorem 1, $\mathbf{0} \in \mathbf{T}_K^{(1)}$ if and only if there is some point $\mathbf{x}_K'$, such that the perpendicular bisector of the line segment $\mathbf{x}_K\mathbf{x}_K'$ passes $\mathbf{0}$. Since $\mathbf{T}_K^{(2)}(\Delta d)$ is the Δd-neighborhood of $\mathbf{T}_K^{(1)}$, $\mathbf{0} \in \mathbf{T}_K^{(2)}(\Delta d)$ if and only if the distance between $\mathbf{0}$ to the perpendicular bisector of the line segment $\mathbf{x}_K\mathbf{x}_K'$ is smaller than Δd. Then, following Case 3 in the proof of [5, Th. 1], $\mathbf{0} \in \mathbf{T}_K^{(2)}(\Delta d)$ if and only if there is some $\mathbf{x}_K'$ located within the following ring region, where (r, θ) denotes the polar coordinate in $\mathbb{R}^2$:

$$S(\Delta d) = \left\{ (r, \theta) \middle| r \geq r_0 \quad \text{and} \quad \left| r^2 - r_0^2 \right| < 2\Delta d \sqrt{r_0^2 + r^2 - 2r_0 r \cos\theta} \right\}. \quad (41)$$

The area of $S(\Delta d)$ is

$$|S(\Delta d)|_2 = 8\Delta d r_0 + O(\Delta d^2). \quad (42)$$

Given the K closest BSs, the point process of the other BSs, denoted as Φ_K^c, is a PPP with intensity 0 in $\mathcal{B}(\mathbf{0}, r_0)$ and intensity λ in $\mathcal{B}_c(\mathbf{0}, r_0)$, due to the strong Markovian property of a PPP. $\mathbb{P}\left(\mathbf{0} \in \mathbf{T}_K^{(2)}(\Delta d) | R_K = r_0\right)$ is equal to the probability that there is at least one point of Φ_K^c in $S(\Delta d)$. Thus we have

$$\begin{aligned} \mathbb{P}\left(\mathbf{0} \in \mathbf{T}_K^{(2)}(\Delta d) | R_K = r_0\right) &= 1 - \exp\left(-\lambda |S(\Delta d)|_2\right) \\ &= 8\lambda \Delta d r_0 + O(\Delta d^2), \end{aligned} \quad (43)$$

which completes the proof. □

C. Proof of Theorem 3

Proof: The probability density function of the distance between the reference user and its Kth closest BS R_K is [34]

$$f_K(r) = \frac{2(\lambda\pi r^2)^K}{r\Gamma(K)} \exp(-\lambda\pi r^2). \quad (44)$$

Then, we have

$$\begin{aligned} &\mathbb{P}(\mathbf{0} \in \mathbf{T}_K^{(2)}(\Delta d)) \\ &= \int_0^\infty \mathbb{P}\left(\mathbf{0} \in \mathbf{T}_K^{(2)}(\Delta d) | R_K = r_0\right) f_K(r_0) \mathrm{d}r_0 \\ &= \frac{8\Gamma\left(\frac{1}{2} + K\right)\sqrt{\lambda}\Delta d}{\Gamma(K)\sqrt{\pi}} + O(\Delta d^2), \end{aligned} \quad (45)$$

which completes the proof. □

D. Proof of Theorem 4

Proof: We aim to show that

$$-\frac{\Delta H(K+1)}{\Delta L(K+1)} + \frac{\Delta H(K)}{\Delta L(K)} > 0, \quad (46)$$

which is equivalent to

$$\Delta H(K)\Delta L(K+1) - \Delta L(K)\Delta H(K+1) > 0. \quad (47)$$

Following the definitions in (27) and (28), (47) is equivalent to

$$\ln\left(\frac{K + 2 - \frac{\alpha}{2}}{K+1}\right) - \frac{K + \frac{1}{2}}{K+1} \ln\left(\frac{K + 1 - \frac{\alpha}{2}}{K}\right) > 0. \quad (48)$$

Through Taylor expansion, we have

$$\ln\left(\frac{K + 2 - \frac{\alpha}{2}}{K+1}\right) = -\sum_{n=1}^{\infty} \frac{\left(\frac{\alpha}{2} - 1\right)^n}{n(K+1)^n}, \quad (49)$$

and

$$\frac{K + \frac{1}{2}}{K+1} \ln\left(\frac{K + 1 - \frac{\alpha}{2}}{K}\right) = -\frac{K + \frac{1}{2}}{K+1} \left(\sum_{n=1}^{\infty} \frac{\left(\frac{\alpha}{2} - 1\right)^n}{nK^n} \right). \quad (50)$$

Since $\frac{\alpha}{2} - 1 > 0$ (i.e., $\alpha > 2$), $\forall n \geq 1$, we have

$$-\frac{\left(\frac{\alpha}{2} - 1\right)^n}{n(K+1)^n} + \frac{K + \frac{1}{2}}{K+1} \left(\frac{\left(\frac{\alpha}{2} - 1\right)^n}{nK^n} \right) > 0. \quad (51)$$

Therefore, (48) is verified, which completes the proof. □

REFERENCES

[1] J. G. Andrews *et al.*, "What will 5G be?" *IEEE J. Sel. Areas Commun.*, vol. 32, no. 6, pp. 1065–1082, Jun. 2014.

[2] N. Lee, D. Morales-Jimenez, A. Lozano, and R. W. Heath, Jr., "Spectral efficiency of dynamic coordinated beamforming: A stochastic geometry approach," *IEEE Trans. Wireless Commun.*, vol. 14, no. 1, pp. 230–241, Jan. 2015.

[3] R. Tanbourgi, S. Singh, J. G. Andrews, and F. K. Jondral, "A tractable model for noncoherent joint-transmission base station cooperation," *IEEE Trans. Wireless Commun.*, vol. 13, no. 9, pp. 4959–4973, Sep. 2014.

[4] X. Lin, R. K. Ganti, P. J. Fleming, and J. G. Andrews, "Towards understanding the fundamentals of mobility in cellular networks," *IEEE Trans. Wireless Commun.*, vol. 12, no. 4, pp. 1686–1698, Apr. 2013.

[5] W. Bao and B. Liang, "Stochastic geometric analysis of user mobility in heterogeneous wireless networks," *IEEE J. Sel. Areas Commun.*, vol. 33, no. 10, pp. 2212–2225, Oct. 2015.

[6] S. Sadr and R. S. Adve, "Handoff rate and coverage analysis in multi-tier heterogeneous networks," *IEEE Trans. Wireless Commun.*, vol. 14, no. 5, pp. 2626–2638, May 2015.

[7] W. Bao and B. Liang, "Handoff rate analysis in heterogeneous wireless networks with Poisson and Poisson cluster patterns," in *Proc. ACM MobiHoc*, Hangzhou, China, Jun. 2015, pp. 77–86.
[8] F. Baccelli and A. Giovanidis, "A stochastic geometry framework for analyzing pairwise-cooperative cellular networks," *IEEE Trans. Wireless Commun.*, vol. 14, no. 2, pp. 794–808, Feb. 2015.
[9] K. Huang and J. G. Andrews, "An analytical framework for multicell cooperation via stochastic geometry and large deviations," *IEEE Trans. Inf. Theory*, vol. 59, no. 4, pp. 2501–2516, Apr. 2013.
[10] S. Akoum and R. W. Heath, "Interference coordination: Random clustering and adaptive limited feedback," *IEEE Trans. Signal Process.*, vol. 61, no. 7, pp. 1822–1834, Apr. 2013.
[11] A. Giovanidis, L. D. A. Corrales, and L. Decreusefond, "Analyzing interference from static cellular cooperation using the nearest neighbour model," in *Proc. IEEE Modeling Optim. Mobile, Ad Hoc, Wireless Netw. (WiOpt)*, Mumbai, India, May 2015, pp. 576–583.
[12] W. Nie, F.-C. Zheng, X. Wang, W. Zhang, and S. Jin, "User-centric cross-tier base station clustering and cooperation in heterogeneous networks: Rate improvement and energy saving," *IEEE J. Sel. Areas Commun.*, vol. 34, no. 5, pp. 1192–1206, May 2016.
[13] G. Nigam, P. Minero, and M. Haenggi, "Coordinated multipoint joint transmission in heterogeneous networks," *IEEE Trans. Commun.*, vol. 62, no. 11, pp. 4134–4146, Nov. 2014.
[14] C. Li, J. Zhang, M. Haenggi, and K. B. Letaief, "User-centric intercell interference nulling for downlink small cell networks," *IEEE Trans. Commun.*, vol. 63, no. 4, pp. 1419–1431, Apr. 2015.
[15] P. Xia, C.-H. Liu, and J. Andrews, "Downlink coordinated multi-point with overhead modeling in heterogeneous cellular networks," *IEEE Trans. Wireless Commun.*, vol. 12, no. 8, pp. 4025–4037, Aug. 2013.
[16] F. Ashtiani, J. A. Salehi, and M. R. Aref, "Mobility modeling and analytical solution for spatial traffic distribution in wireless multimedia networks," *IEEE J. Sel. Areas Commun.*, vol. 21, no. 10, pp. 1699–1709, Dec. 2003.
[17] Y.-C. Chen, J. Kurose, and D. Towsley, "A mixed queueing network model of mobility in a campus wireless network," in *Proc. IEEE INFOCOM*, Orlando, FL, USA, Mar. 2012, pp. 2656–2660.
[18] A. Farbod and B. Liang, "Structured admission control policy in heterogeneous wireless networks with mesh underlay," in *Proc. IEEE INFOCOM*, Rio de Janeiro, Brazil, Apr. 2009, pp. 495–503.
[19] W. Bao and B. Liang, "Insensitivity of user distribution in multicell networks under general mobility and session patterns," *IEEE Trans. Wireless Commun.*, vol. 12, no. 12, pp. 6244–6254, Dec. 2013.
[20] T. S. Rappaport, *Wireless Communications: Principles and Practice*, 2nd ed. Englewood Cliffs, NJ, USA: Prentice-Hall, 2002.
[21] A. S. Anpalagan and I. Katzela, "Overlaid cellular system design, with cell selection criteria for mobile wireless users," in *Proc. IEEE Can. Conf. Elect. Comput. Eng.*, Edmonton, AB, Canada, May 1999, pp. 24–28.
[22] N. Shenoy and B. Hartpence, "A mobility model for cost analysis in integrated cellular/WLANs," in *Proc. Int. Conf. Comput. Commun. Netw.*, Chicago, IL, USA, Oct. 2004, pp. 275–280.
[23] A. Hasib and A. O. Fapojuwo, "Mobility model for heterogeneous wireless networks and its application in common radio resource management," *IET Commun.*, vol. 2, no. 9, pp. 1186–1195, Oct. 2008.
[24] W. Bao and B. Liang, "Stochastic geometric analysis of handoffs in user-centric cooperative wireless networks," in *Proc. IEEE INFOCOM*, San Francisco, CA, USA, Apr. 2016, pp. 1–9.
[25] M. Haenggi, J. G. Andrews, F. Baccelli, O. Dousse, and M. Franceschetti, "Stochastic geometry and random graphs for the analysis and design of wireless networks," *IEEE J. Sel. Areas Commun.*, vol. 27, no. 7, pp. 1029–1046, Sep. 2009.
[26] F. Baccelli and B. Blaszczyszyn, "Stochastic geometry and wireless networks, volume 1: Theory," *Found. Trends Netw.*, vol. 3, nos. 3–4, pp. 249–449, 2009.
[27] F. Baccelli and B. Blaszczyszyn, "Stochastic geometry and wireless networks, volume 2: Applications," *Found. Trends Netw.*, vol. 4, nos. 1–2, pp. 1–312, 2009.
[28] M. Haenggi, *Stochastic Geometry for Wireless Networks*. Cambridge, MA, USA: Cambridge Univ. Press, 2012.
[29] D. Stoyan, W. Kendall, and J. Mecke, *Stochastic Geometry and Its Applications*, 2nd ed. Hoboken, NJ, USA: Wiley, 1995.
[30] H. Federer, *Geometric Measure Theory*. Berlin, Germany: Springer, 1969.
[31] *Coordinated Multi-Point Operation for LTE Physical Layer Aspects*, document 3GPP-TR-36.819, Sep. 2013.
[32] A. M. Ibrahim, T. ElBatt, and A. El-Keyi, "Coverage probability analysis for wireless networks using repulsive point processes," in *Proc. IEEE PIMRC*, London, U.K., Sep. 2013, pp. 1002–1007.
[33] A. Guo and M. Haenggi, "Spatial stochastic models and metrics for the structure of base stations in cellular networks," *IEEE Trans. Wireless Commun.*, vol. 12, no. 11, pp. 5800–5812, Nov. 2013.
[34] M. Haenggi, "On distances in uniformly random networks," *IEEE Trans. Inf. Theory*, vol. 51, no. 10, pp. 3584–3586, Oct. 2005.

Wei Bao received the B.E. degree in communications engineering from the Beijing University of Posts and Telecommunications, Beijing, China, in 2009, the M.A.Sc. degree in electrical and computer engineering from The University of British Columbia, Vancouver, Canada, in 2011, and the Ph.D. degree in electrical and computer engineering from the University of Toronto, Toronto, Canada, in 2016. He is currently a Lecturer with the School of Information Technologies, The University of Sydney, Sydney, Australia. His research covers the area of network science, with particular emphasis on 5G systems, Internet of Things, and mobile computing. He received the best paper awards at the ACM International Conference on Modeling, Analysis and Simulation of Wireless and Mobile Systems in 2013 and the IEEE International Symposium on Network Computing and Applications in 2016.

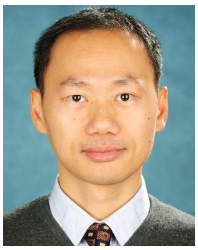

Ben Liang (SM'06) received the B.Sc. (Valedictorian) degree (Hons.) and the M.Sc. degree in electrical engineering from Polytechnic University, Brooklyn, NY, USA, in 1997, and the Ph.D. degree in electrical engineering with a minor in computer science from Cornell University, Ithaca, NY, USA, in 2001. In 2001 and 2002, he was a Visiting Lecturer and a Post-Doctoral Research Associate with Cornell University. He joined the Department of Electrical and Computer Engineering, University of Toronto, in 2002, where he is currently a Professor. His current research interests are in networked systems and mobile communications. He is a member of ACM and Tau Beta Pi. He regularly serves on the organizational and technical committees of a number of conferences. He was an Editor of the IEEE TRANSACTIONS ON WIRELESS COMMUNICATIONS from 2008 to 2013 and an Associate Editor of *Security and Communication Networks* (Wiley) from 2007 to 2016. He has been serving on the editorial boards of the IEEE TRANSACTIONS ON MOBILE COMPUTING since 2017 and the IEEE TRANSACTIONS ON COMMUNICATIONS since 2014.